Geologia Croatica
Journal of the Croatian Geological Survey and the Croatian Geological Society
2026 | 79/3 | 291–300 | 6 Figs. | 4 Tabs. | 2 Suppls. | www.geologia-croatica.hr

Clinopyroxene thermobarometry of the Çatak pillow basalts, Maden Complex (Eastern Anatolia): Implications for magma storage conditions and mantle melting

Tijen Üner[1,*]

[1,*] Department of Geological Engineering, Van Yüzüncü Yıl University, Tuşba, Van, Türkiye; (correspondig author: tcakici@yyu.edu.tr)

doi: 10.4154/gc.2026.13

CC BY
Crossref Similarity Check

Original scientific paper

Article history:
Manuscript received: February 19, 2026
Revised manuscript accepted: July 20, 2026
Available online: October 14, 2026

Abstract

The tectonomagmatic affinity of the Maden Complex within the southeastern Anatolian orogenic belt remains debated, with interpretations ranging from intra-oceanic arc and back-arc basin development to post-collisional and MORB-type mantle derivation. However, quantitative mineral-scale constraints on magma storage conditions are limited. This study presents new clinopyroxene major-element data from submarine pillow basalts exposed in the Çatak area (Eastern Anatolia) and applies established clinopyroxene-based thermobarometric formulations to constrain crystallization pressures and temperatures. Clinopyroxenes are compositionally restricted to the augite field and display moderate Mg# values (≈ 68–77), with negligible calculated Fe^{3+} contents, indicating relatively reduced crystallization conditions. Discrimination diagrams show dominant E-MORB to ocean-floor basalt affinities, without systematic Ti depletion, typical of strongly fluid-fluxed arc-front settings. Thermobarometric calculations yield crystallization temperatures of ≈ 1100–1190 °C and pressures predominantly between ≈ 4–8 kbar, consistent with intermediate crustal magma storage conditions. The inferred pressure–temperature regime is compatible with crystallization from basaltic melts derived from spinel-facies mantle sources proposed in previous regional studies. Integration of mineral chemistry and thermobarometric data suggests magma evolution under transitional MORB-like to supra-subduction extensional conditions. These results provide new quantitative constraints on the mantle melting regime and magma storage depth in the Çatak segment and support the interpretation of tectonomagmatic heterogeneity within the Maden Complex.

Keywords: Clinopyroxene thermobarometry, pressure-temperature constraints, Maden Complex, submarine basalts, Neotethys; Eastern Anatolia

1. INTRODUCTION

The southeastern Anatolian orogenic belt represents a critical segment of the Alpine–Himalayan collisional system and preserves key geological records of the Late Cretaceous to Cenozoic evolution and closure of the southern branch of the Neotethys Ocean. This region is characterized by the tectonic juxtaposition of ophiolitic mélanges, volcanic-sedimentary successions, and platform carbonates, reflecting a complex history of oceanic spreading, intra-oceanic subduction, nappe emplacement, and subsequent continental collision (ŞENGÖR &YILMAZ, 1981; ROBERTSON et al., 2012). Within this framework, the Maden Complex constitutes one of the most debated tectonomagmatic assemblages in terms of its stratigraphic definition, mantle source characteristics, and geodynamic significance. The complex has also been interpreted as part of a Neotethyan active continental margin system comprising accretionary wedge units, ophiolitic slices, and arc-related volcanic assemblages, assembled during Late Cretaceous–Palaeogene subduction (AKTAŞ & ROBERTSON, 1984).

The term "Maden Complex" has historically been applied to lithologically diverse volcanic and sedimentary units exposed along the Bitlis–Zagros suture zone, resulting in considerable stratigraphic and tectonic ambiguity. Based on detailed field mapping and stratigraphic relationships, YİĞİTBAŞ & YILMAZ (1996) redefined the Maden Group sensu stricto as a Middle Eocene volcano-sedimentary succession developed within a short-lived back-arc basin that evolved toward an embryonic oceanic stage. In this model, transitional to tholeiitic basalts were interpreted as products of incipient oceanic spreading within a supra-subduction extensional regime. This interpretation emphasized basin development behind an active arc and suggested that localized oceanic crust formation may have occurred during the Eocene evolution of the southeastern Anatolian domain.

Subsequent geochemical and isotopic investigations, however, have challenged a simple back-arc interpretation. Whole-rock major-trace element data and Sr–Nd isotope systematics presented by ERTÜRK et al. (2018) suggested that Eocene magmatism within the Maden Complex reflects post-collisional

extension driven by lithospheric thinning and asthenospheric upwelling following continental collision. In this scenario, decompression melting of a subduction-modified mantle source generated basaltic to andesitic magmas without requiring active back-arc spreading. This model shifts the tectonic emphasis from syn-subduction basin development to post-orogenic extensional collapse within the Bitlis–Zagros suture zone.

More recently, mineral-chemical and Sr–Nd–Pb isotopic data from the Malatya sector reported by SAR et al. (2025) indicated derivation of Maden volcanic rocks from a shallow spinel-bearing lherzolitic mantle source with mid ocean ridge basalt (MORB)-like isotopic characteristics. Their results place the studied rocks close to the MORB field in the Sr–Nd–Pb isotope space and emphasize spinel-facies melting conditions at relatively shallow mantle depths. This interpretation further complicates the tectonic classification of the Maden Complex and suggests that mantle source characteristics may vary along strike.

Taken together, these contrasting interpretations – back-arc basin development (YİĞİTBAŞ & YILMAZ, 1996), post-collisional asthenospheric upwelling (ERTÜRK et al., 2018), and MORB-type shallow mantle derivation (SAR et al., 2025) – indicate that the Maden Complex cannot be explained by a single, homogeneous tectonomagmatic model. Instead, the available data point toward significant spatial heterogeneity in mantle melting regimes, magma plumbing architecture, and crustal thickness within different segments of the complex. Notably, most previous studies have relied primarily on whole-rock geochemistry and isotope systematics, whereas independent mineral-scale pressure–temperature constraints remain limited.

Mineral chemistry, particularly clinopyroxene systematics, provides a powerful and independent tool for evaluating mantle source characteristics, melt evolution processes, redox conditions, and crystallization depths in basaltic systems (NIMIS, 1995; PUTIRKA, 2008). Clinopyroxene major-element compositions are sensitive to variations in melt compo-

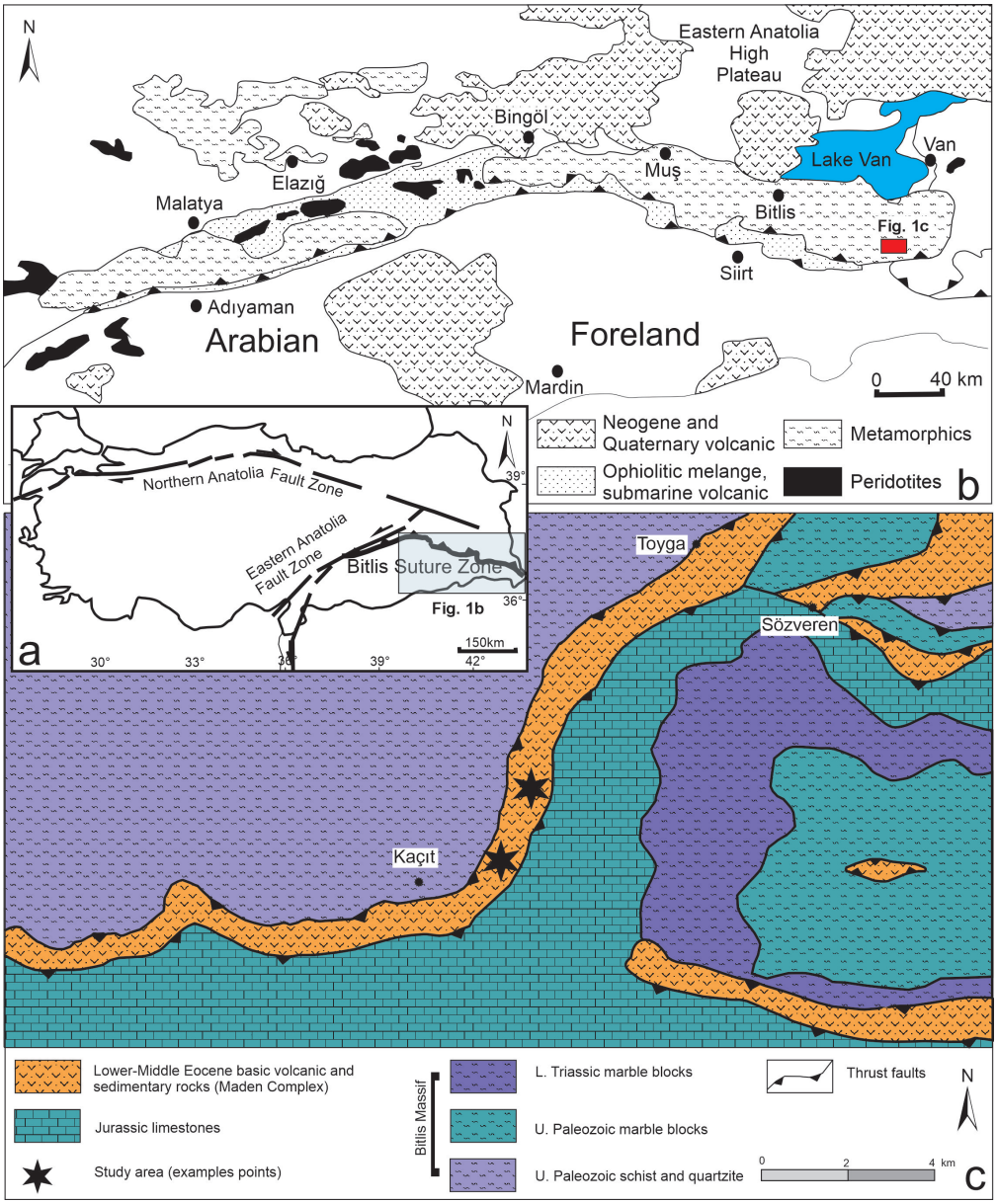


Figure 1. (**a**) Inset location map showing the position of the Bitlis Suture Zone in eastern Türkiye (modified after BOZKURT, 2001); (**b**) Simplified geological map of the eastern Anatolian region showing the location of the Çatak study area within the Maden Complex belt, (modified after BİNGÖL, 1989; ELİTOK & DOLMAZ, 2008); (**c**) Simplified geological map of the Çatak area showing lithological units, thrust contacts, and sample locations.

sition, water content, and pressure-temperature conditions, and therefore can discriminate between MORB-type, arc-related, and transitional supra-subduction magmatic environments. Moreover, clinopyroxene-based thermobarometric formulations enable quantitative reconstruction of magma storage depths and thermal regimes, even where whole-rock compositions may be affected by alteration or seawater interaction.

In this study, we present new clinopyroxene major-element data from well-preserved pillow basalts exposed in the Çatak area (Van region), representing the southern sector of the Maden Complex. We apply established clinopyroxene thermobarometric formulations to quantitatively constrain crystallization pressures and temperatures and to constrain magma storage conditions and crystallization depths. By integrating mineral chemistry with pressure-temperature estimates, this study provides independent mineral-scale constraints on magma storage depth, mantle melting conditions, and tectonomagmatic affinity. In doing so, we evaluate whether the Çatak segment supports a back-arc (YİĞİTBAŞ & YILMAZ, 1996), post-collisional (ERTÜRK et al., 2018), MORB-type shallow mantle (SAR et al., 2025), or transitional supra-subduction interpretation within the evolving southern Neotethyan system.

2. GEOLOGICAL SETTING

The Çatak study area is located in Van Province, southeastern Eastern Anatolia, and forms part of the southern sector of the Eastern Anatolian orogenic belt (Fig. 1). This region constitutes a key segment of the Alpine–Himalayan collisional system and preserves geological records of the Late Cretaceous–Palaeogene evolution and closure of the southern branch of the Neotethys Ocean (ŞENGÖR & YILMAZ, 1981; ROBERTSON et al., 2012).

Regionally, the geology is dominated by ophiolitic and ophiolite-derived units, tectonically emplaced onto the Anatolian continental margin, during northward subduction of Neotethyan oceanic lithosphere and subsequent continental collision between the Arabian and Eurasian plates (ROBERTSON et al., 2012). In the Van–Çatak region, these assemblages include mantle peridotites, gabbros, sheeted dyke complexes, and extensive basaltic volcanic sequences locally preserved as pillow basalts (ÖZDEMİR et al., 2021; MERCAN, 2021).

Geophysical data indicate present-day crustal thicknesses of approximately 40–45 km beneath Eastern Anatolia, with evidence for localized lithospheric thinning and relatively shallow asthenospheric domains (KESKİN, 2007). Although



Figure 2. Field characteristics of the Çatak pillow basalts: (**a**) Laterally continuous pillow lava packages forming thick submarine flow units; (**b**) Decimetre- to metre-scale ellipsoidal pillows with chilled margins and locally developed radial cooling fractures; (**c**) Stacked pillow structures forming massive flow accumulations; (**d**) Irregular pillow contacts and brecciated inter-pillow zones produced by lava-water interaction.

largely related to post-collisional processes, this crustal architecture provides an important framework for evaluating magma storage depths inferred from mineral thermobarometry.

In the study area, basaltic rocks occur predominantly as well-preserved pillow lava flows, indicating submarine eruption. Pillow lavas form thick, laterally continuous flow packages (Fig. 2a, c). The preservation of primary pillow morphologies suggests limited post-emplacement deformation.

Individual pillows are typically ellipsoidal to subrounded and range from decimetre to metre scale. They display fine-grained to glassy chilled margins surrounding more crystalline interiors, and locally exhibit radial cooling fractures (Fig. 2b). Irregular contacts between adjacent pillows and brecciated inter-pillow zones reflect quench fragmentation during lava–water interaction (Fig. 2d), consistent with submarine basaltic volcanism.

Pillow lavas lack a consistent flow orientation; however, their irregular stacking geometry suggests emplacement over an uneven submarine substrate (Fig. 2c–d).

Petrographically, the basalts exhibit porphyritic to microporphyritic textures dominated by clinopyroxene and plagioclase within a fine-grained microlitic groundmass. Representative BSE images reveal intersertal to intergranular textures characterized by plagioclase-rich groundmass surrounding clinopyroxene phenocrysts and microphenocrysts (Fig. 3a–d). Clinopyroxene occurs as euhedral to subhedral crystals and locally displays brittle fracturing and weak internal heterogeneity. Plagioclase is present predominantly as microlitic laths within the groundmass, whereas opaque phases occur as scattered anhedral grains. Olivine was not identified in the studied samples, suggesting either early fractionation or crystallization from relatively evolved basaltic melts (MERCAN, 2021; ÖZDEMİR et al., 2021; ÜNER, 2024). The observed textures are consistent with relatively rapid cooling during submarine emplacement of basaltic lavas.

At the regional scale, the volcanic facies characteristics and petrographic features of the Çatak pillow basalts are consistent with formation in a submarine oceanic environment related to Neotethyan magmatism. Previous studies similarly interpret these units as remnants of Neotethyan oceanic lithosphere with predominantly MORB-like geochemical affinities (ÖZDEMİR et al., 2021; URAL et al., 2021).

In summary, the Çatak pillow basalts represent submarine volcanic products emplaced during Neotethyan oceanic

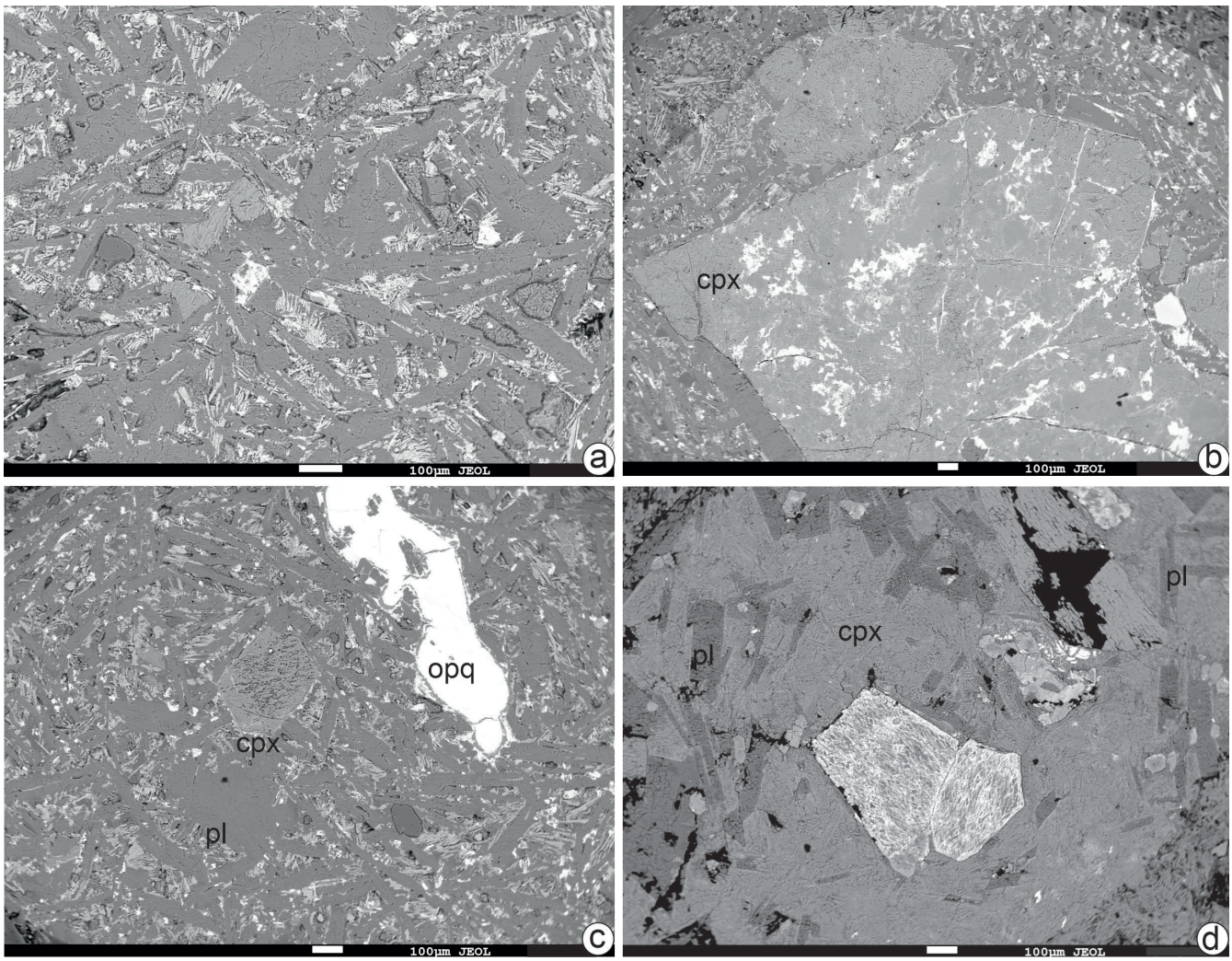


Figure 3. Representative BSE images of the Çatak pillow basalts showing porphyritic to microlitic textures and mineral relationships: (**a**) Microlitic to intersertal groundmass dominated by plagioclase laths; (**b**) Large clinopyroxene phenocryst (Cpx) showing fractured texture within fine-grained groundmass; (**c**) Clinopyroxene phenocryst associated with opaque phases (Opq) and plagioclase microlites (Pl); (**d**) Euhedral to subhedral clinopyroxene phenocrysts (Cpx) surrounded by plagioclase-rich microlitic groundmass (Pl).

magmatism prior to ophiolite obduction and continental collision, providing the geological framework for subsequent mineral-chemical and thermobarometric analysis.

3. MATERIALS AND METHODS

Major-element compositions of clinopyroxene were determined using a JEOL JXA-8230 Electron Probe Micro Analyzer (EPMA) equipped with five wavelength-dispersive spectrometers (WDS) at the Earth Sciences Application and Research Center, Ankara University. Polished thin sections were carbon-coated prior to analysis. Analytical conditions included an accelerating voltage of 20 kV and a beam current of 20 nA. Natural mineral and oxide standards supplied by Micro-Analysis Consultants Ltd. (MAC) were used for calibration. Matrix corrections were performed using the ZAF procedure implemented in the JEOL software, accounting for atomic number (Z), absorption (A), and fluorescence (F) effects. Analytical precision for major elements is estimated to be within ± 1–2 %.

Clinopyroxene structural formulae were recalculated on the basis of 6 oxygens per formula unit (Table 1, Table S1), and Fe^{3+} contents were estimated using the charge-balance method of DROOP (1987). End-member components (Wo–En–Fs) and Mg# values were calculated as $Mg/(Mg+Fe^{2+}) \times 100$ using recalculated cation proportions. Mg# values recalculated using Fe^{2+} are systematically higher than values calculated using total Fe.

The clinopyroxene-liquid equilibrium was evaluated using Fe–Mg exchange coefficients following PUTIRKA (2008). Only analyses satisfying $KD(Fe–Mg) = 0.27 \pm 0.03$ were retained for thermobarometric calculations. Pressure and temperature estimates were primarily calculated using the clinopyroxene-liquid thermobarometer of PUTIRKA (2008) (Table 2; Table S2). Additional pressure estimates were calculated using the formulations of NIMIS (1995) and NIMIS & ULMER (1998) for comparison. The XPT–YPT parameters were calculated following SOESOO (1997) for the independent estimation of crystallization pressure and temperature. Major-element-based F1–F2 discrimination parameters were calculated using the functions of LETERRIER et al. (1982).

Whole-rock compositions (CB-1 and CB-2) were used as approximate melt proxies in thermobarometric calculations due to the absence of fresh volcanic glass in the pillow basalts. Although the relatively evolved nature of these whole-rock

Table 1. Representative electron microprobe analyses and recalculated structural formulae of clinopyroxenes from the Çatak pillow basalts. Complete dataset is provided in Supplementary Table S1.

No.	CB1_1	CB1_2	CB1_3	CB1_8	CB1_12	CB1_13	CB2_12	CB2_22	CB2_23	CB2_29	CB2_33
SiO_2	50.94	51.29	48.90	49.87	51.05	50.60	50.29	50.63	50.60	50.32	51.48
TiO_2	2.03	2.11	2.10	2.49	1.98	2.05	2.04	1.73	1.83	1.97	1.85
Al_2O_3	4.36	4.02	3.77	4.07	2.90	3.94	4.08	3.78	3.53	3.80	5.24
FeO	10.21	9.16	9.81	12.02	9.86	11.35	10.83	9.67	10.34	10.31	9.47
MnO	0.17	0.15	0.09	0.16	0.18	0.16	0.15	0.16	0.15	0.15	0.11
MgO	12.72	13.26	14.04	16.02	14.61	15.73	15.39	14.77	14.90	15.06	12.68
CaO	18.56	18.91	20.15	14.34	18.49	15.43	16.36	18.41	17.67	17.40	18.77
Na_2O	0.80	0.81	0.51	0.82	0.83	0.62	0.75	0.49	0.60	0.64	0.11
K2O	0.01	0.00	0.01	0.01	0.00	0.00	0.01	0.01	0.01	0.01	0.01
Cr_2O_3	0.09	0.04	0.02	0.04	0.02	0.03	0.05	0.08	0.05	0.07	0.03
Total	99.80	99.72	99.39	99.80	99.89	99.87	99.89	99.65	99.62	99.65	99.72
Si	1.898	1.905	1.846	1.859	1.903	1.880	1.871	1.886	1.889	1.877	1.904
Ti	0.057	0.059	0.060	0.070	0.055	0.057	0.057	0.048	0.051	0.055	0.052
Al^{IV}	0.102	0.095	0.154	0.141	0.097	0.120	0.129	0.114	0.111	0.123	0.096
Al^{VI}	0.089	0.081	0.014	0.038	0.030	0.053	0.049	0.052	0.044	0.044	0.133
Altotal	0.191	0.176	0.168	0.179	0.127	0.173	0.179	0.166	0.155	0.167	0.229
Fe^{2+}	0.318	0.285	0.310	0.375	0.307	0.353	0.337	0.301	0.323	0.322	0.293
Mn	0.005	0.005	0.003	0.005	0.006	0.005	0.005	0.005	0.005	0.005	0.004
Mg	0.706	0.734	0.790	0.890	0.811	0.871	0.854	0.820	0.829	0.837	0.699
Ca	0.741	0.753	0.815	0.573	0.738	0.614	0.652	0.735	0.707	0.695	0.744
Na	0.058	0.058	0.038	0.059	0.060	0.045	0.054	0.035	0.044	0.047	0.008
K	0.000	0.000	0.001	0.000	0.000	0.000	0.000	0.000	0.000	0.000	0.001
Cr	0.003	0.001	0.000	0.001	0.000	0.001	0.001	0.002	0.002	0.002	0.001
Sum	3.978	3.976	4.029	4.011	4.008	3.998	4.009	3.999	4.004	4.007	3.933
Fe^{3+}	0.000	0.000	0.058	0.021	0.017	0.000	0.018	0.000	0.007	0.013	0.000
Mg#	69.00	72.00	72.00	70.00	73.00	71.00	72.00	73.00	72.00	72.00	70.00
Wo	41.8	42.4	41.2	30.7	39.3	33.3	35.0	39.5	37.8	37.1	42.8
En	39.9	41.3	40.0	47.8	43.2	47.3	45.8	44.1	44.3	44.7	40.2
Fs	18.3	16.3	18.8	21.5	17.5	19.4	19.3	16.5	17.9	18.1	17.0

Table 2. Representative clinopyroxene thermobarometric estimates calculated using the formulations of PUTIRKA (2008). Complete thermobarometric dataset, including alternative formulations, is provided in Supplementary Table S2.

Sample No		P (kbar)	T(°C)	Kd(Fe-Mg)
	1	8.16	1175.61	0.28
	3	4.87	1100.02	0.26
CB 1	8	5.95	1160.32	0.27
	12	2.44	1171.85	0.27
	15	9.67	1200.05	0.28
	2	1.72	1094.44	0.25
	6	6.79	1194.57	0.27
CB 2	12	2.22	1104.11	0.26
	18	6.88	1184.36	0.27
	29	4.65	1227.10	0.27

compositions may introduce uncertainty into absolute pressure estimates, they provide first-order constraints on crystallization conditions.

4. RESULTS

4.1. Clinopyroxene Mineral Chemistry

Clinopyroxenes display a restricted compositional range consistent with crystallization from basaltic melts. SiO_2 contents range from 49.1–52.9 wt.%, TiO_2 from 0.23–2.49 wt.%, and Al_2O_3 from 1.4–5.2 wt.%. Total FeO_t varies between 7.8 and 12.4 wt.%, and Cr_2O_3 <0.15 wt.% (Table 1, Table S1).

Structural formulae for clinopyroxenes were recalculated on the basis of 6 oxygens and 4 cations per formula unit. Calculated Si values range between 1.84 and 1.97 a.p.f.u., indicating limited tetrahedral Al substitution. Total Al contents (0.08–0.23 a.p.f.u.) are distributed between Al^{IV} and Al^{VI} sites, reflecting coupled substitution mechanisms typical of basaltic clinopyroxenes (MORIMOTO, 1988; DEER et al., 2013). Mg values range between 0.70 and 0.94 a.p.f.u., whereas total Fe contents vary from 0.25 to 0.39 a.p.f.u. Mg# values range from ≈ 68 to 77 Table 1, Table S1).

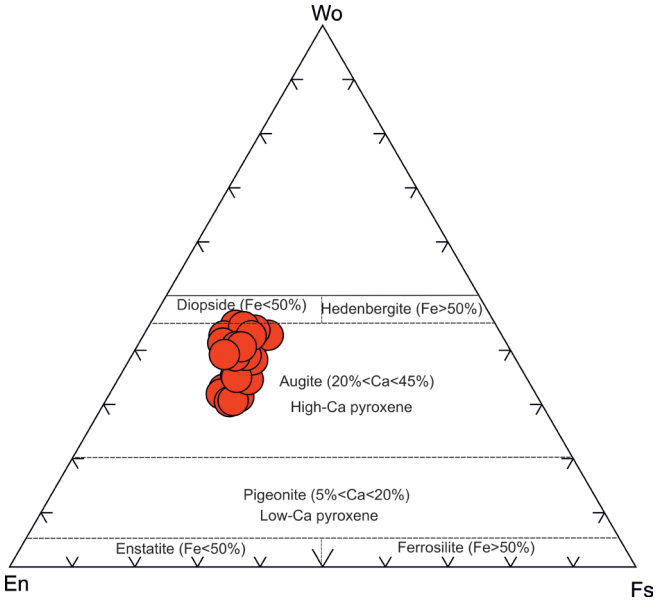


Figure 4. Pyroxene ternary (En–Fs–Wo) illustrating compositional fields for enstatite–ferrosilite (low-Ca), pigeonite, augite (high-Ca), and the diopside–hedenbergite join; red circles represent analyzed clinopyroxene compositions.

Fe–Mg exchange coefficients (KD ≈ 0.27 ± 0.03) are consistent with clinopyroxene–liquid equilibrium according to the criteria of PUTIRKA (2008). Charge-balance calculations following DROOP (1987) indicate generally low calculated Fe^{3+} contents (Table 1, Table S1).

In the Wo–En–Fs classification diagram (MORIMOTO, 1988), all analyses plot within the high-Ca clinopyroxene field (augite), with minor overlap toward the diopside field (Fig. 4). No compositions plot within low-Ca pyroxene fields.

In Ti–(Ca+Na) and (Cr+Ti)–Ca discrimination diagrams (LETERRIER et al., 1982), most analyses cluster within basalt-related compositional fields (Fig. 5a–b). Clinopyroxene discrimination diagrams based on TiO_2–SiO_2/100–Na_2O, F1–F2 and Al_2O_3 versus TiO_2+Cr_2O_3 systematics are shown in Fig. 5c–e. The tectonomagmatic significance of these distributions is discussed in Section 5.1.

4.2. Clinopyroxene Thermobarometry

The Al^{VI} + 2Ti + Cr versus Al^{VI} + Na diagram (SCHWEITZER et al., 1979) places most clinopyroxene analyses within the high oxygen-fugacity field (Fig. 6a). In the AlIV–AlVI discrimination diagram, most analyses cluster near the low-pressure igneous field boundary, although significant scatter limits precise pressure discrimination (Fig. 6b).

Clinopyroxene–liquid equilibrium was evaluated using the Fe–Mg exchange coefficient of PUTIRKA (2008), and only analyses satisfying KD(Fe–Mg) = 0.27 ± 0.03 were retained for thermobarometric calculations (Table 2, Table S2).

Pressure and temperature estimates calculated using the clinopyroxene–liquid thermobarometer of PUTIRKA (2008) indicate crystallization pressures broadly ranging between ≈ 4 and 8 kbar (≈ 0.4–0.8 GPa), although several analyses extend toward lower-pressure conditions (Fig. 6c). Calculated temperatures vary between ≈ 1100 and 1190 °C.

Additional pressure estimates obtained using the formulations of NIMIS (1995) and NIMIS & ULMER (1998) show greater scatter relative to the PUTIRKA (2008) calculations (Table 2, Table S2).

5. DISCUSSION

5.1. Assessment of Arc and MORB Affinities

Discriminating between arc-related, back-arc, and ridge-type magmatism requires evaluation of mantle source modification, redox state, and melt evolution processes. Clinopyroxene chemistry is particularly sensitive to these parameters because Ti, Al, and Fe systematics respond directly to slab-fluid metasomatism, oxygen fugacity, and melt water content (LETERRIER et al., 1982; PEARCE & PEATE, 1995; PUTIRKA, 2008).

In subduction-zone settings, slab-derived aqueous fluids preferentially mobilize large-ion lithophile elements while leaving HFSE relatively immobile, commonly generating Ti-depleted melts derived from a metasomatized mantle wedge (PEARCE & PEATE, 1995; PEARCE & STERN, 2006). Experimental and geochemical studies further indicate that slab-derived fluids may transfer oxidizing components into the mantle wedge, producing relatively oxidized arc magmas

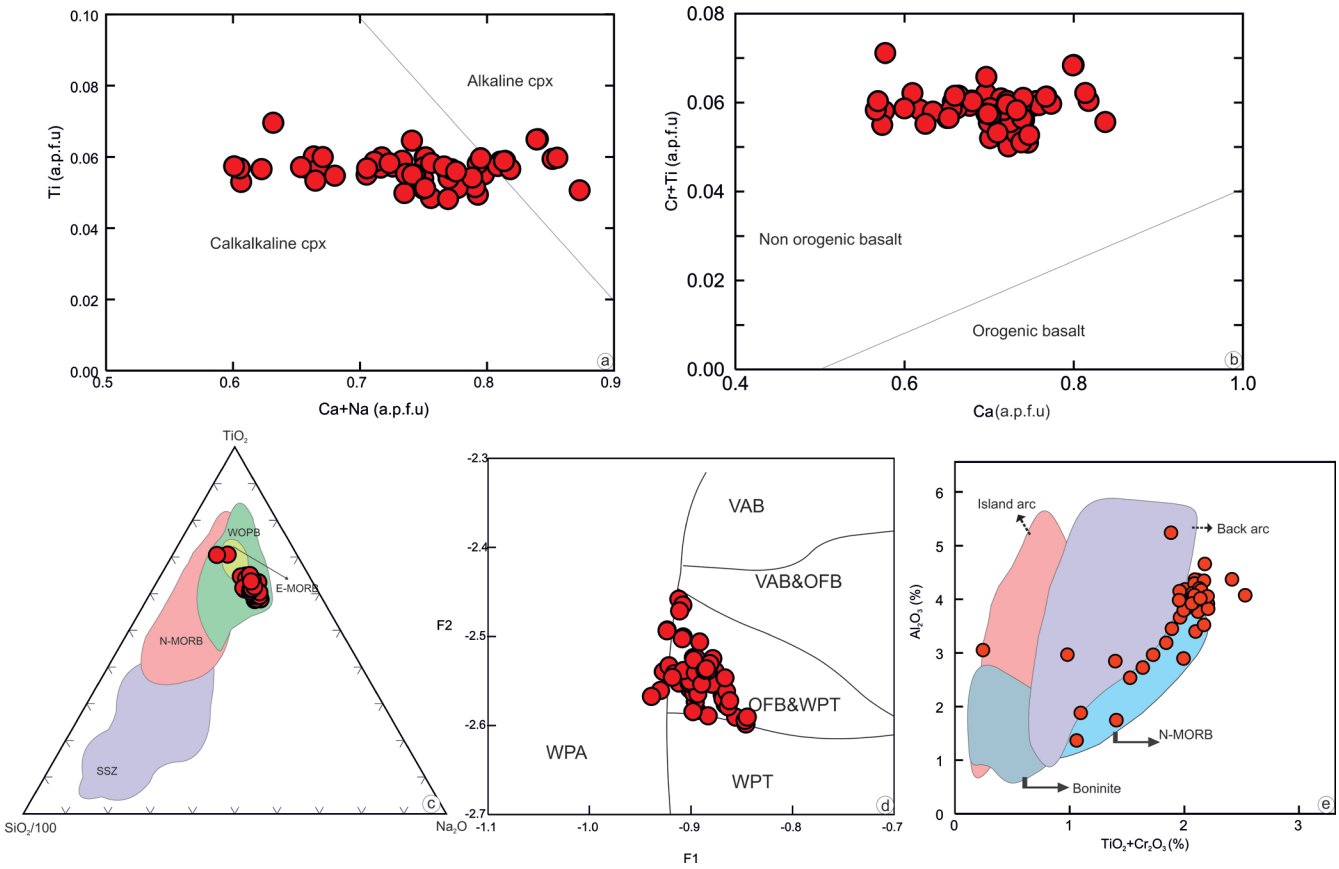


Figure 5. Clinopyroxene-based tectonomagmatic discrimination diagrams: (**a**) Ti vs. (Ca+Na) and (**b**) Cr+Ti vs. Ca diagrams after LETERIRIER et al. (1982), distinguishing alkaline and calc-alkaline affinities as well as non-orogenic and orogenic basalt fields; (**c**) TiO_2–Na_2O–SiO_2/100 ternary discrimination diagram after BECCALUVA et al. (1989), showing MORB (N-MORB and E-MORB), WPOB and SSZ domains; (**d**) F1 vs. F2 discrimination diagram after NISBET & PEARCE (1977), separating VAB (volcanic arc basalt), OFB (ocean floor basalt), WPT (within-plate tholeiite) and WPA (within-plate alkaline) fields. The discrimination functions used for panel d are: F1=[(–0.012*SiO_2) – (0.0807*TiO_2) + (0.0026*Al_2O_3) – (0.0012*FeO) – (0.0026* MnO) + (0.0087*MgO) – (0.0128*CaO) – (0.0419*Na_2O)]; F2= [(–0.0469*SiO_2) – (0.0818*TiO_2) – (0.0212*Al_2O_3) – (0.0041*FeO) – (0.1435*MnO) – (0.0029*MgO) + (0.0085*CaO) + (0.0160*Na_2O)]; (**e**) Al_2O_3 versus TiO_2+Cr_2O_3 discrimination diagram for clinopyroxenes from the Çatak pillow basalts after HOUT et al., 2002. Most analyses plot within the back-arc affinity field with partial overlap toward MORB-related domains.

(KELLEY & COTTRELL, 2009; CANNAÒ & MALASPINA, 2018). Such processes typically produce clinopyroxenes characterized by suppressed Ti contents and coherent clustering within volcanic arc basalt fields.

The Çatak clinopyroxenes do not display systematic Ti depletion and predominantly plot within basalt-related compositional fields in Ti–(Ca+Na) and (Cr+Ti)–Ca space (Fig. 5a–b). This absence of strong HFSE suppression suggests limited slab-fluid modification during magma evolution beneath the Çatak segment.

Redox conditions provide an additional constraint on magma evolution. Although the $Al^{VI} + 2Ti + Cr$ versus $Al^{VI} + Na$ diagram places most analyses within the high oxygen-fugacity field (Fig. 6a), the Çatak clinopyroxenes do not display the pronounced Ti depletion typically associated with strongly fluid-fluxed arc-front magmas. Likewise, calculated Fe^{3+} contents are generally low and do not clearly indicate the strongly oxidized conditions commonly associated with arc-front magmatism.

Water content and crystallization pressure further differentiate arc and non-arc environments. Experimental studies demonstrate that hydrous, high-pressure arc magmas promote elevated tetrahedral Al incorporation in clinopyroxene (GAETANI & GROVE, 1998; PUTIRKA, 2008). The Çatak dataset does not show systematic enrichment in tetrahedral Al, suggesting crystallization from relatively low- to moderate-water basaltic melts rather than strongly hydrous arc magmas (Fig. 6b).

In contrast, MORB and extensional supra-subduction environments are commonly associated with extensional melting regimes and limited slab-fluid modification (PEARCE & PEATE, 1995; ISHIZUKA et al., 2020). Consistent with this framework, the majority of clinopyroxene compositions cluster within the E-MORB field in the TiO_2–SiO_2/100–Na_2O ternary diagram (Fig. 5c), whereas F1–F2 discrimination places most samples within the OFB field with limited dispersion toward adjacent compositional domains (Fig. 5d). Likewise, the Al_2O_3 versus TiO_2+Cr_2O_3 discrimination diagram (HOUT et al., 2002) indicates a predominant back-arc affinity with partial overlap into MORB-related compositions (Fig. 5e).

The combined mineral-chemical characteristics therefore indicate predominantly MORB-like affinities with transitional back-arc characteristics and limited to moderate slab-fluid influence. However, clinopyroxene discrimination diagrams principally constrain mantle source characteristics and crystallization conditions; they do not uniquely identify the geodynamic mechanism driving extension. Accordingly, the observed mineral-scale signatures are considered compatible

Geologia Croatica

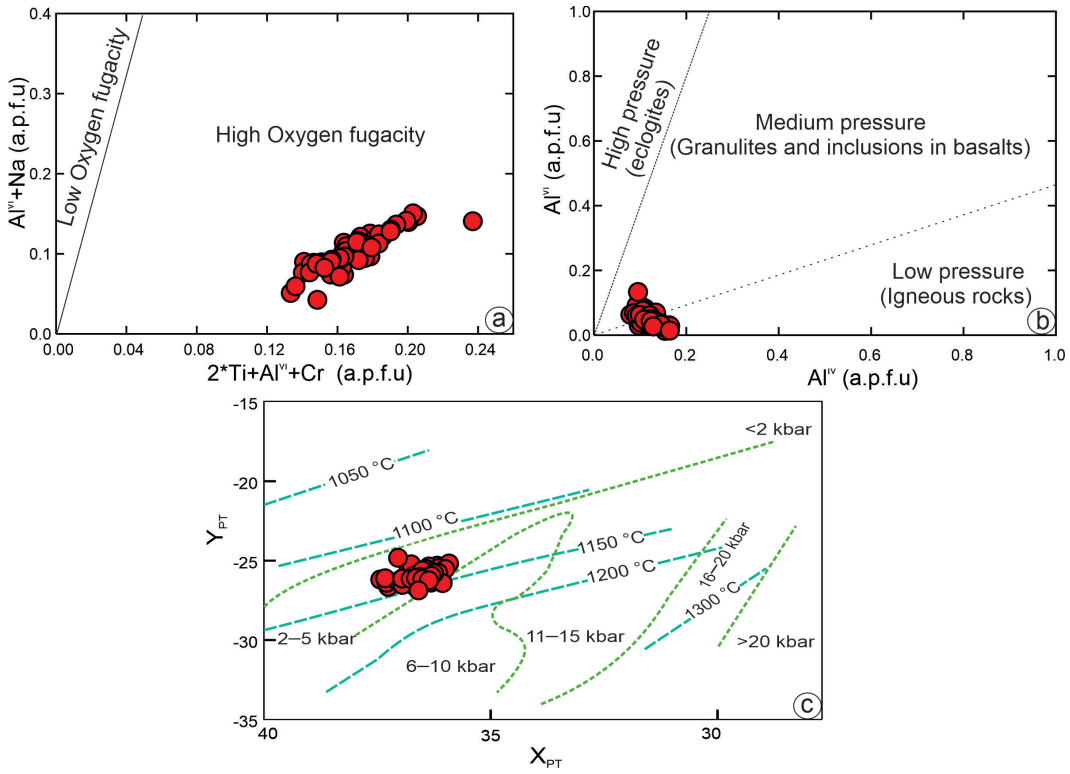


Figure 6. Clinopyroxene redox and thermobarometric diagrams for the Çatak pillow basalts: (**a**) $Al^{VI} + 2Ti + Cr$ vs. $Al^{VI} + Na$ (a.p.f.u.) diagram for oxygen fugacity estimation (after SCHWEITZER et al., 1979); (**b**) Al^{VI} vs. Al^{IV} (a.p.f.u.) barometry diagram distinguishing pressure-sensitive crystallization fields (after AOKI & SHIBA, 1973); (**c**) X_{PT}–Y_{PT} diagram for estimating crystallization pressure and temperature of pyroxenes (after SOESOO, 1997). $X_{PT} = [(0.446*SiO_2) + (0.187*TiO_2) – (0.404*Al_2O_3) + (0.346*FeO_t) – (0.052*MnO) + (0.309*MgO) + (0.431*CaO) – (0.446*Na_2O)]$; $Y_{PT} = [(–0.369*SiO_2) + (0.535*TiO_2) – (0.317*Al_2O_3) + (0.323*FeO_t) + (0.235*MnO) – (0.516*MgO) – (0.167*CaO) – (0.153*Na_2O)]$.

with extensional supra-subduction and/or back-arc-related magmatism previously proposed for the Maden Complex (YİĞİTBAŞ & YILMAZ, 1996; ERTÜRK et al., 2018), rather than evidence for a single homogeneous tectonomagmatic regime.

5.2. Pressure-Temperature Regime of the Çatak Magmatic System

Clinopyroxene-based thermobarometry provides important constraints on crystallization conditions and magma storage levels within basaltic systems. Accordingly, clinopyroxene thermobarometric formulations were applied to evaluate the pressure–temperature (P-T) conditions of the Çatak pillow basalts.

Pressure-temperature estimates were calculated using the clinopyroxene–liquid equilibrium equations of PUTIRKA (2008), employing whole-rock compositions CB-1 and CB-2 (ÜNER, 2024) as approximate melt proxies due to the absence of fresh volcanic glass (Table 2). Although the relatively evolved nature of these whole-rock compositions may introduce uncertainty into absolute pressure estimates, the calculated values provide first-order constraints on crystallization conditions. Previous studies have emphasized that thermobarometric estimates may vary depending on calibration range, melt composition, and equilibrium assumptions (PUTIRKA, 2008; TILL, 2017). The PUTIRKA (2008) formulation was preferred here because it yielded the most internally consistent results within the compositional range of the analyzed clinopyroxenes.

Clinopyroxene-melt equilibrium was evaluated using KD(Fe–Mg) = 0.27 ± 0.03, and only equilibrium-compatible analyses were retained for thermobarometric calculations (Table 2). Alternative barometers (NIMIS, 1995; NIMIS & ULMER, 1998) produced more scattered pressure estimates relative to the PUTIRKA (2008) calculations, likely reflecting differences in calibration sensitivity, equilibrium assumptions, and melt-composition dependence, particularly where whole-rock compositions are used as melt proxies instead of fresh glass compositions. Estimated uncertainties are approximately ± 1.5–2 kbar for pressure and ± 30–50 °C for temperature, consistent with ranges discussed in previous thermobarometric assessments (PUTIRKA, 2008; TILL, 2017).

In the Al^{IV}–Al^{VI} discrimination diagram, most clinopyroxene analyses cluster near the low-pressure igneous field boundary, although significant scatter limits precise pressure discrimination (Fig. 6b). Similarly, the $Al^{VI} + 2Ti + Cr$ versus $Al^{VI} + Na$ diagram (SCHWEITZER et al., 1979) places most analyses within the high oxygen-fugacity field (Fig. 6a). However, the clinopyroxene compositions do not display the pronounced Ti depletion typically associated with strongly fluid-fluxed arc-front magmas.

Putirka-derived pressures broadly range between ≈ 4 and 8 kbar, although several analyses extend toward lower-pressure conditions (Fig. 6c; Table 2). Calculated temperatures vary from ≈ 1100 to 1190 °C, consistent with crystallization from basaltic melts under relatively low- to moderate-water conditions. The obtained pressure range is broadly compatible with

magma storage at intermediate crustal levels prior to submarine eruption.

The calculated pressures do not support extremely shallow ridge-axis magma chambers (≈ 1–3 km; WHITE et al., 2006; RUBIN & SINTON, 2007), but they also do not indicate deep arc-root crystallization conditions (>10–12 kbar) typical of thickened island-arc crust (ANNEN et al., 2006). Consequently, the thermobarometric dataset is most consistent with intermediate-pressure crystallization conditions prior to eruption.

5.3. Tectonomagmatic Implications for the Maden Complex

The Maden Complex has long been interpreted as an accretionary wedge–arc system developed along the southern Neotethyan margin based on regional stratigraphic and structural relationships (AKTAŞ & ROBERTSON, 1984). The clinopyroxene mineral chemistry and thermobarometric results presented here provide additional constraints on the crystallization conditions and magmatic affinity of the Çatak pillow basalts.

Thermobarometric calculations suggest crystallization at intermediate crustal levels, broadly corresponding to pressures of ≈ 4–8 kbar and temperatures of ≈ 1100–1190 °C (Fig. 6c; Table 2). The calculated pressure range does not support extremely shallow ridge-axis magma chambers, nor does it indicate deep arc-root crystallization conditions typical of thickened island-arc crust (ANNEN et al., 2006; WHITE et al., 2006; RUBIN & SINTON, 2007). Collectively, these observations are most consistent with intermediate-pressure crystallization prior to submarine eruption.

Clinopyroxene compositions are restricted mainly to augite and display moderate Mg# values (≈ 68–77). In tectonomagmatic discrimination diagrams, most analyses cluster within MORB-related to transitional supra-subduction fields (Fig. 5a–d). In addition, the Al_2O_3 versus TiO_2+Cr_2O_3 discrimination diagram (HOUT et al., 2002) places most analyses within the back-arc affinity field, with partial overlap toward MORB-related compositions (Fig. 5e). Although such discrimination diagrams do not uniquely constrain tectonic setting, the combined mineral-chemical characteristics indicate predominantly MORB-like affinities with transitional back-arc characteristics and limited to moderate slab-fluid influence.

Taken together, the clinopyroxene chemistry and thermobarometric data are compatible with magma evolution in an extensional supra-subduction and/or back-arc-related magmatic environment. In this context, previously proposed models involving back-arc extension (YİĞİTBAŞ & YILMAZ, 1996), post-collisional extension (ERTÜRK et al., 2018), and MORB-like mantle affinities (SAR et al., 2025) may reflect variable magmatic conditions within different segments of the Maden Complex rather than mutually exclusive tectonic regimes.

The principal contribution of this study is the provision of mineral-scale crystallization constraints for the Çatak pillow basalts using clinopyroxene chemistry and thermobarometry. These results provide additional quantitative constraints on magma storage conditions and magmatic affinity within the southern sector of the Maden Complex.

6. CONCLUSION

This study presents new clinopyroxene major-element data and thermobarometric estimates for the Çatak pillow basalts of the Maden Complex. The integrated mineral-chemical and pressure–temperature dataset provides additional constraints on crystallization conditions and magmatic affinity within the southern sector of the Maden Complex.

The principal conclusions are as follows:

1. Clinopyroxene compositions are restricted mainly to augite and display moderate Mg# values (≈ 68–77). In tectonomagmatic discrimination diagrams, most analyses cluster within MORB-related to transitional back-arc/supra-subduction affinity fields.
2. The clinopyroxene compositions do not show systematic Ti depletion typically associated with strongly fluid-fluxed arc-front magmas, suggesting limited to moderate slab-fluid influence during magma evolution.
3. Clinopyroxene-based thermobarometry (PUTIRKA, 2008) yields crystallization pressures broadly between ≈ 4 and 8 kbar and temperatures of ≈ 1100–1190 °C. Although the evolved nature of the whole-rock melt proxies introduces uncertainty into absolute pressure estimates, the results provide first-order constraints on crystallization conditions.
4. The obtained pressure-temperature conditions are compatible with magma storage at intermediate crustal levels prior to submarine eruption.
5. Combined mineral-chemical and thermobarometric data are consistent with magma evolution in an extensional supra-subduction to back-arc magmatic environment.

Within the broader framework of the Maden Complex, these results support the interpretation that magmatic conditions may have varied along different segments of the Neotethyan domain. The present study provides mineral-scale constraints that contribute to understanding the crystallization conditions and magmatic affinity of the Çatak pillow basalts.

REFERENCES

AKTAŞ, G. & ROBERTSON, A.H.F. (1984): The Maden Complex, SE Turkey: evolution of a Neotethyan active margin.- Geological Society, London, Special Publications, 17, 375–401. https://doi.org/10.1144/GSL.SP.1984.017.01.27

ANNEN, C., BLUNDY, J.D. & SPARKS, R.S.J. (2006): The genesis of intermediate and silicic magmas in deep crustal hot zones.– Journal of Petrology, 47, 505–539. https://doi.org/10.1093/petrology/egi084

AOKI, K.I. & SHIBA, I. (1973): Pyroxenes from lherzolites inclusions of Itinonagata, Japan. Lithos, 6, 41–51. https://doi.org/10.1016/0024-4937(73)90078-9

BECCALUVA L., MACCIOTTA G., PICCARDO, G.B. & ZEDA, O. (1989): Clinopyroxene composition of ophiolite basalts as petrogenetic indicator.– Chemical Geology, 77, 165–182.

BİNGÖL, E. (1989): Geological map of Turkey (Scale: 1:2 000 000).– General Directorate of Mineral Research and Exploration (MTA), Ankara, Turkey.

BOZKURT, E. (2001): Neotectonics of Turkey—a synthesis.– Geodinamica Acta, 14, 3–30.

CANNAÒ, E. & MALASPINA, N. (2018): From oceanic to continental subduction: Implications for the oxidation state of the mantle wedge.– Geosphere, 14/6, 2311–2336. https://doi.org/10.1130 /GES01597.1

DEER, W.A., HOWIE, R.A. & ZUSSMAN, J. (2013): An Introduction to the Rock-Forming Minerals.– Mineralogical Society, London, 498 p. https://doi.org/10.1180/DHZ

DROOP, G.T.R. (1987): A general equation for estimating Fe^{3+} concentrations in ferromagnesian silicates.– Mineralogical Magazine, 51, 431–435. https://doi.org/10.1180/ minmag.1987.051.361.10

ELİTOK, Ö. & DOLMAZ, M.N. (2008): Mantle flow-induced crustal thinning in the area between the easternmost part of the Anatolian plate and the Arabian Foreland (E Turkey) deduced from the geological and geophysical data.– Gondwana Research, 13, 302–318. https://doi.org/10.1016/j.gr.2007.08.007

ERTÜRK, M.A., BEYARSLAN, M., CHUNG, S-L. & LIN, T-H. (2018): Eocene magmatism (Maden Complex) in the Southeast Anatolian Orogenic Belt: Magma genesis and tectonic implications.– Geoscience Frontiers, 9, 1829–1847. https://doi.org/10.1016/j.gsf.2017.09.008

GAETANI, G.A. & GROVE, T.L. (1998): The influence of water on melting of mantle peridotite.– Contributions to Mineralogy and Petrology, 131, 323–346. https://doi.org/10.1007/ s004100050396

HOUT, F., HÉBERT, R., VARFALVY, V., BEAUDOIN, G.,WANG, C.S., LIU, Z.F., COTTEN, J. & DOSTAL, J. (2002): The Beimarang Melange (Southern Tibet) brings additional constraints in assessing the origin, metamorphic evolution and obduction processes of the Yarlung Zangbo Ophiolite.– Journal of Asian Earth Sciences 21, 307–22.

ISHIZUKA, O., TAYLOR, R.N., UMINO, S. & KANAYAMA, K. (2020): Geochemical evolution of arc and slab following subduction initiation: a record from the Bonin Islands, Japan.– Journal of Petrology, 61/5, egaa050. https://doi.org/10.1093/ petrology/ egaa050

KELLEY, K.A. & COTTRELL, E. (2009): Water and the oxidation state of subduction zone magmas.– Science, 325, 5940, 605–607. https://doi.org/10.1126/science.1174156

KESKİN, M. (2007): Eastern Anatolia: A hotspot in a collision zone without a mantle plume.- Geological Society of America Special Papers, 430, 693–722. https://doi.org/10.1130/2007.2430(32)

LETERRIER, J., MAURY, R.C., THONON, P., GIRARD, D. & MARCHAL, M. (1982): Clinopyroxene composition as a method of identification of magmatic affinities.– Earth and Planetary Science Letters, 59/1, 139–154. https://doi.org/10.1016/0012-821X(82)90122-4

MERCAN, Ç. (2021): Geological and petrological characteristics of the Maden Complex volcanics exposed between Çatak (Van) and Kozluk (Batman), Eastern Türkiye.– Doctoral dissertation, Van Yüzüncü Yıl University, Graduate School of Natural and Applied Sciences, Department of Geological Engineering, Van, Türkiye, 235p.

MORIMOTO, N. (1988): Nomenclature of pyroxenes.- Mineralogy and Petrology, 39, 55–76. https://doi.org/10.1007/BF01226262

NIMIS, P. & TAYLOR, W.R. (2000): Single clinopyroxene thermobarometry.- Contributions to Mineralogy and Petrology, 139, 541–554. https://doi.org/10.1007/s004100000156

NIMIS, P. & ULMER, P. (1998): Clinopyroxene geobarometry of magmatic rocks Part 1: An expanded structural geobarometer for anhydrous and hydrous, basic and ultrabasic systems.- Contributions to Mineralogy and Petrology, 133, 122–135. https://doi.org/10.1007/s004100050442

NIMIS, P. (1995): A clinopyroxene geobarometer for basaltic systems.– Contributions to Mineralogy and Petrology, 121, 115–125. https://doi.org/10.1007/s004100050093

NISBET, E.G., & PEARCE, J.A. (1977): Clinopyroxene Composition in Mafic Lavas from Different Tectonic Settings.– Contributions to Mineralogy and Petrology, 63, 149-160. https://doi.org/10.1007/bf00398776

ÖZDEMİR, Y., GÜLEÇ, N., ÖZKAN ALTINER, S., OYAN, V., ÖZDEMİR, A. (2021): Petrological, sedimentological and paleontological characteristics of the Middle Eocene Maden Complex rocks (Çatak–Kozluk): Implications for the closure of the southern branch of the Neotethys Ocean.– Unpublished project report (TÜBİTAK Project No. 117Y355, Program 1001), The Scientific and Technological Research Council of Türkiye (TÜBİTAK), Ankara, Türkiye, 235p.

PEARCE, J.A. & PEATE, D.W. (1995): Tectonic implications of the composition of volcanic arc magmas.– Annual Review of Earth and Planetary Sciences, 23, 251–285. https://doi.org/10.1146/annurev.ea.23.050195.001343

PEARCE, J.A. & STERN, R.J. (2006): Origin of back-arc basin magmas: Trace element and isotopic perspectives.– In: PEARCE, J.A. & STERN, R.J. (eds.): Back-Arc Spreading Systems: Geological, Biological, Chemical, and Physical Interactions.– Geophysical Monograph Series, 166, 63–86. https://doi.org/10.1029/166GM06

PUTIRKA, K.D. (2008): Thermometers and barometers for volcanic systems.– Reviews in Mineralogy and Geochemistry, 69/1, 61–120. https://doi.org/10.2138/rmg.2008.69.3

ROBERTSON, A.H.F., PARLAK, O. & USTAÖMER, T. (2012): Overview of the Palaeozoic–Neogene evolution of Neotethys in the Eastern Mediterranean region.– Geological Society, London, Special Publications, 18, 381–404. https://doi.org/ 10.1144/petgeo2011-091

RUBIN, K.H. & SINTON, J.M. (2007): Inferences on mid-ocean ridge magma chamber processes from MORB chemistry.– Earth and Planetary Science Letters, 260, 257–276. https://doi.org/10.1016/j.epsl.2007.05.035

SAR, A., RIZELI, M.E., ERTÜRK, M.A. & YILMAZ, İ. (2025): Petrogenesis of the Maden Complex volcanic rocks in the southeastern Anatolian orogenic belt.– In: EGU General Assembly Conference Abstracts, EGU25-8091. https://doi.org/10.5194/egusphere-egu25-8091

SCHWEITZER, E., PAPIKE, J. & BENCE, A. (1979): Statistical analysis of clinopyroxenes from deep-sea basalts.– American Mineralogist, 64, 501–513.

SOESOO, A. (1997): A multivariate statistical analysis of clinopyroxene composition: empirical coordinates for the crystallisation PT-estimations. GFF, 119, 55–60. 10.1080/11035899709546454

URAL, M. SAYİT, K., KORALAY, O.E. & GÖNCÜOĞLU, M.C. (2021): Geochemistry and Zircon U-Pb Dates of Felsic-Intermediate Members of the Late Cretaceous Yüksekova Arc Basin: Constraints on the Evolution of the Bitlis–Zagros Branch of Neotethys (Elazığ, E Turkey).– Acta Geologica Sinica, 95/4, 1199–1216. https://doi.org/10.1111/1755-6724.14694

ÜNER, T. (2024): Maden Karmaşığı'ndaki (Çatak-Van) Yastık Yapılı Bazaltların Kökeni: Petrografik ve Jeokimyasal Yaklaşım [*Origin of pillow basalts in the Maden Complex (Çatak–Van): Petrographic and geochemical approach* – in Turkish].– Yerbilimleri/ Earth Sciences, 45, 227–246. https://doi.org/10.17824/yerbilimleri.1440128

TILL, C.B. (2017): A review and update of mantle thermobarometry for primitive arc magmas.– American Mineralogist, 102/5, 931–947. https://doi.org/10.2138/am-2017-5783

WHITE, S.M., CRISP, J.A. & SPERA, F.J. (2006): Long-term volumetric eruption rates and magma budgets.– Geochemistry, Geophysicis, Geosystems, 7/3, Q03010, https://doi.org/10.1029/2005GC001002

YİĞİTBAŞ, E. & YILMAZ, Y. (1996): New evidence and solution to the Maden Complex controversy of the southeast Anatolian orogenic belt (Turkey).– Geologische Rundschau, 85, 250–263. https://doi.org/10.1007/BF02422232

Electronic supplementary material is available online at
http://www.geologia-croatica.hr